The Journal of Chemical Physics

RESEARCH ARTICLE | APRIL 08 2019

Understanding the anharmonic vibrational structure of the carbon dioxide dimer FREE

Samuel Maystrovsky; Murat Keçeli ; Olaseni Sode

J. Chem. Phys. 150, 144302 (2019)
https://doi.org/10.1063/1.5089460
CHORUS

AIP Publishing

The Journal of Chemical Physics ARTICLE scitation.org/journal/jcp

Understanding the anharmonic vibrational structure of the carbon dioxide dimer

Cite as: J. Chem. Phys. 150, 144302 (2019); doi: 10.1063/1.5089460
Submitted: 18 January 2019 • Accepted: 19 March 2019 •
Published Online: 8 April 2019

Samuel Maystrovsky,[1] Murat Keçeli,[2] and Olaseni Sode[1,3,a)]

AFFILIATIONS

[1] Department of Chemistry, Biochemistry and Physics, The University of Tampa, 401 West Kennedy Boulevard, Tampa, Florida 33606, USA
[2] Computational Science Division, Argonne National Laboratory, Lemont, Illinois 60439, USA
[3] Department of Chemistry and Biochemistry, California State University, Los Angeles, 5151 State University Drive, Los Angeles, California 90032, USA

[a)] **Author to whom correspondence should be addressed:** osode@calstatela.edu

ABSTRACT

Understanding the vibrational structure of the CO_2 system is important to confirm the potential energy surface and interactions in such van der Waals complexes. In this work, we use our previously developed *mb*CO2 potential function to explore the vibrational structure of the CO_2 monomer and dimer. The potential function has been trained to reproduce the potential energies at the CCSD(T)-F12b/aug-cc-pVTZ level of electronic structure theory. The harmonic approximation, as well as anharmonic corrections using vibrational structure theories such as vibrational self-consistent field, vibrational second-order Møller-Plesset perturbation, and vibrational configuration interaction (VCI), is applied to address the vibrational motions. We compare the vibrational results using the *mb*CO2 potential function with traditional electronic structure theory results and to experimental frequencies. The anharmonic results for the monomer most closely match the experimental data to within 3 cm^{-1}, including the Fermi dyad frequencies. The intermolecular and intramolecular dimer frequencies were treated separately and show good agreement with the most recent theoretical and experimental results from the literature. The VCI treatment of the dimer vibrational motions accounts for vibrational mixing and delocalization, such that we observe the dimer Fermi resonance phenomena, both in the intramolecular and intermolecular regions.

I. INTRODUCTION

The extensive amount of scientific interest in the carbon dioxide molecule is due to the monumental impact it has on our everyday lives. Most notably, CO_2 is a major greenhouse gas and thus a significant cause of anthropogenic climate change. Also supercritical CO_2 plays an important role in industrial applications as an environmentally friendly solvent. Crucial to understanding these processes is understanding the intra- and intermolecular interactions that govern this molecule. In particular, the weak van der Waals interactions are quite difficult to describe but are necessary to explore large scale interactions such as in clusters or in the condensed phase. Vibrational spectroscopy represents one of the most sensitive techniques to probe these relatively weak interactions. This approach, in all of its different forms, can provide necessary information about the potential energy surface (PES) of the complexes including the rotational and vibrational dynamics and vibrational band shifts upon complexation, all of which provide insight into the underlying chemistry of the CO_2 system.

The vibrational degrees of freedom of the isolated carbon dioxide molecule have been extensively studied with a variety of spectroscopic experimental methods.[1–6] The monomer has four normal modes of vibration including the symmetric stretching mode, ν_1, the asymmetric stretching mode, ν_3, and two degenerate bending modes, ν_2 and $\nu_{\bar{2}}$, which have been precisely identified in the literature. Even the accidental degeneracy of the symmetric stretch fundamental and the first bending overtone (the textbook example of Fermi resonance) has been explored at length in the experimental literature.[7–12] Likewise, the dimer has long been the focus of experimental investigations, mainly by infrared spectroscopy.[13–17] What is

especially interesting about this system is the large-amplitude intermolecular vibrations. The four fundamental intermolecular dimer modes are the antisymmetric in-plane bend (ν_a), the out-of-plane torsion (ν_b), the symmetric van der Waals stretch (ν_c), and the symmetric in-plane bend (ν_d). These motions are particularly difficult to interpret since they exist in the low-frequency terahertz region of the vibrational spectrum, and until recently, the experimental data here were sparse. However, in the past few years, Moazzen-Ahmadi and co-workers have described five intermolecular vibrations for this species using a combination of theoretical and experimental data.[18,19]

Theoretical studies on the vibrational structure of the isolated CO_2 monomer are as numerous as experimental studies. Often, a quartic force field (QFF) PES, constructed at various levels of electronic structure theory, is used to explore this system.[20–25] To date, however, the best theoretical results were obtained with a Gauss-Hermite quadrature grid using a PES computed at the coupled cluster singles and double with perturbative triples [CCSD(T)]/complete basis set (CBS) limit and accounting for vibrational anharmonicity.[25] At this level of theory for the monomer, the vibrational energy levels, including the Fermi dyad peak positions, were determined to within only a few wavenumbers of the experimental band assignments. For the CO_2 dimer, several theoretical techniques have been used to describe the complex vibrational spectrum.[26–30] Specifically, Bukowski *et al.* determined the intermolecular vibrational frequencies using a PES derived from symmetry-adapted perturbation theory.[31] Also, the seminal paper by Chen and Light used a discrete variable representation (DVR) in a spherical harmonic basis to address these large-amplitude motions.[32] Most recently, Wang *et al.* generated a rigid-monomer four-dimensional CO_2 dimer PES calculated at the (AE)-CCSD(T*)-F12b/CVQZ-F12 level and employed a DVR basis to determine the anharmonic vibrational structure of the intermolecular motions.[33] Their results were used to help identify the combination bands in the asymmetric stretching region of the infrared spectrum.[19] The majority of the literature work for the dimer is restricted to the rigid monomer motions and lacks a flexible monomer treatment. As such there are few results that describe the intramolecular region of the CO_2 dimer.

Recently, one of the current authors developed a flexible-monomer two-body potential energy function (PEF) for carbon dioxide.[34] This new potential, termed *mb*CO2, was constructed by fitting permutationally invariant polynomials to CO_2 monomer and dimer configurations calculated at the CCSD(T)-F12b/aug-cc-pVTZ level of electronic structure theory. This procedure has recently shown to be effective at accurately describing the PES for many small molecular systems, including water,[35–39] methane,[40] and the hydronium ion[41] to name a few. Here, the *mb*CO2 potential has been shown to accurately predict the PES of small clusters of CO_2 much larger than the dimer and thus is appropriate to predict the vibrational structure of CO_2 systems as well. Again, given the sensitivity to not only the relative energy but also the shape of the PES, vibrational structure prediction points toward the true accuracy of the PES.

The most straightforward vibrational structure approach is the harmonic approximation since it treats each normal coordinate as a non-interacting harmonic oscillator. This framework provides a reference solution, which neglects both the anharmonicity in the one-dimensional PES and the coupling between vibrational degrees of freedom. Fortunately, modern vibrational structure methods, especially those that explicitly treat the correlation between modes (vibrational correlation methods), can remedy this deficiency. These methods, including vibrational self-consistent field (VSCF) theory, vibrational second-order Møller-Plesset perturbation (VMP2) theory, and vibrational configuration interaction (VCI) theory, are constructed in similar ways to their electronic structure counterparts and represent a hierarchy of increasing accuracy. The choice of coordinate space is also crucial for an accurate depiction of the vibrational degrees of freedom. In most cases, rectilinear (Cartesian) coordinates can be employed. This choice is especially effective when addressing rigid intramolecular motions; however, the slow, floppy motions of the intermolecular region are best described by curvilinear coordinates.[42–46] In this work, we use both internal and Cartesian coordinates to separately treat the large-amplitude low-frequency motions and the rigid intramolecular vibrations, respectively. This article focuses on combining these existing methods with the recently developed *mb*CO2 potential in order to fully understand the vibrational structure of the carbon dioxide monomer and dimer. We also employ a hierarchy of vibrational structure methods paired with different PES approximations in order to make the most accurate predictions of the vibrational frequencies.

II. METHODOLOGY

A. Potential energy surface

The majority of the potential energy calculations in this work were performed with a variant of the previously developed flexible-monomer two-body potential function, *mb*CO2.[34] Instead of the fifth-degree polynomial function used for two-body interactions, however, a slightly less flexible, fourth-degree polynomial potential energy function (PEF) was employed. This substitution was due to two factors: (1) the new PEF is more efficient, which, given the number of CO_2 energy calculations, amounts to a substantial speedup and (2) the fourth-degree polynomial is smoother, ensuring the higher numerical derivative terms are stable and non-divergent. This new PEF can be found in the supplementary material. Contour plots of the dimer PES are shown in Fig. 1 along the four characteristic coordinates (θ_1, θ_2, ϕ, R), where the global energy minimum is found at $\theta_1 = \theta_2 = 58.3°$, $\phi = 0°$, and R = 3.66 Å. The CO_2 monomer and dimer were optimized using this potential, and the harmonic vibrational frequencies were obtained. For both the geometry optimizations and the vibrational frequency calculations, numerical energy derivatives were performed with the central difference approach and a step size of 5.0×10^{-3} Å. Also, *ab initio* electronic structure calculations at the CCSD(T)-F12b level of theory were performed on the carbon dioxide monomer and dimer with the aug-cc-pVQZ basis sets using the MOLPRO software package.[47] Again, each of these molecules was optimized, after which the harmonic frequencies were numerically calculated.

For the vibrational structure calculations, we approximated the full PES of the CO_2 monomer and dimer using both a quartic force field (QFF) and Gauss-Hermite quadrature (grid). The QFF is defined as a Taylor series expansion of the minimum energy geometry truncated after fourth-order and is written as

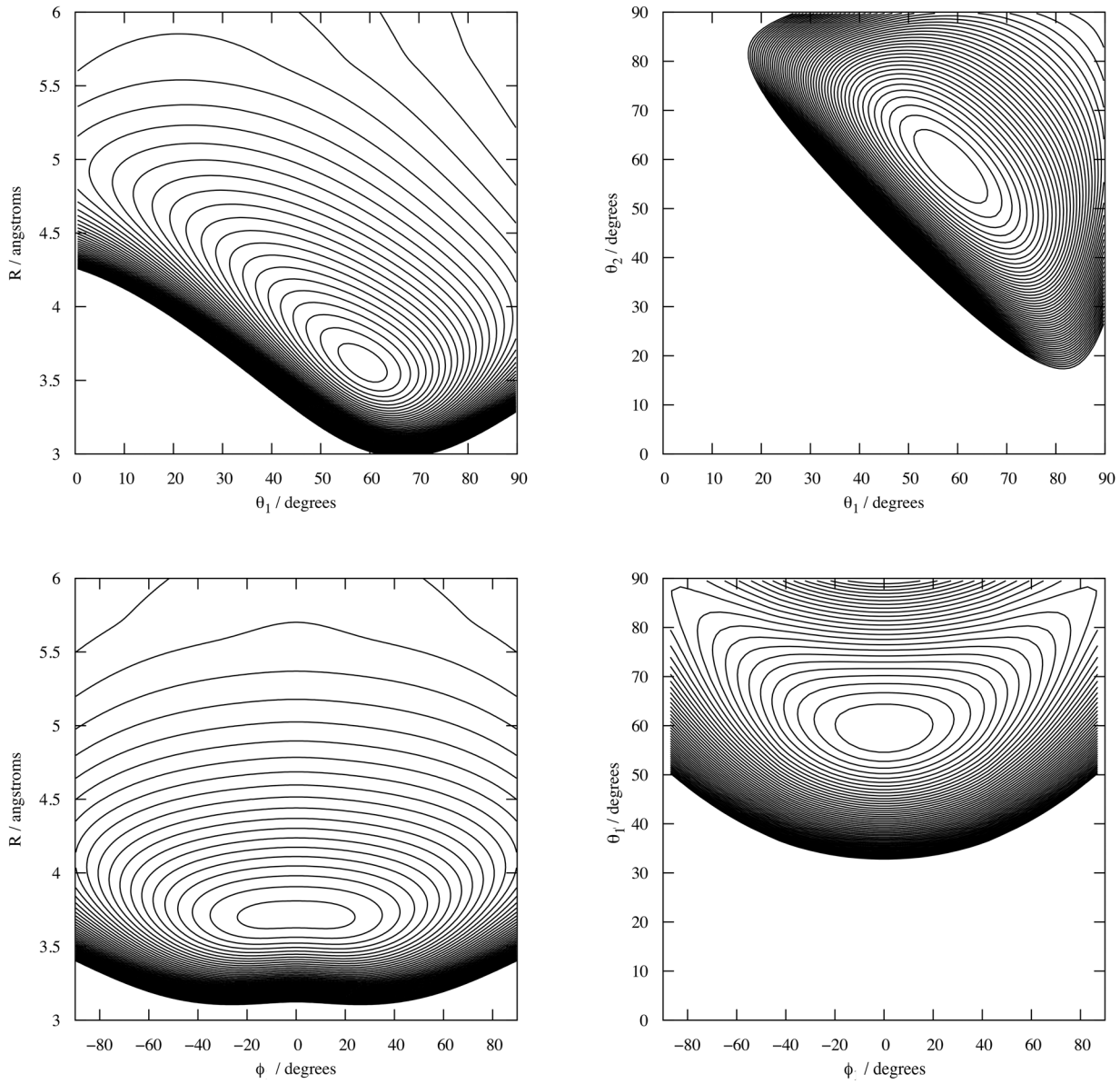

FIG. 1. Intermolecular potential energy surface of the CO_2 dimer near the minimum energy structure (−522.8 cm^{-1}) with a contour spacing of 20 cm^{-1}. The fourth degree *mb*CO2 potential function[34] was used. In each plot, all other coordinates, including the intramolecular bond distances, are held fixed.

$$V^{\mathrm{QFF}} = V_0 + \sum_{i}^{n} g_i Q_i + \frac{1}{2}\sum_{ij}^{n} h_{ij} Q_i Q_j + \frac{1}{6}\sum_{ijk}^{n} t_{ijk} Q_i Q_j Q_k + \frac{1}{24}\sum_{ijkl}^{n} u_{ijkl} Q_i Q_j Q_k Q_l. \quad (1)$$

The Q_m terms represent the mth normal coordinate, and the units are in Å $u^{1/2}$. The g_i, h_{ij}, t_{ijk}, and u_{ijkl} terms represent the linear, quadratic, cubic, and quartic force constants, respectively. These were obtained numerically using the *mb*CO2 potential with a step size of 5.0×10^{-3} Å. One, two, and three mode coupling representations (1MR, 2MR, and 3MR, respectively) were also employed. The Gauss-Hermite quadrature representation takes the following form:

$$V^{\mathrm{Grid}} = \sum_{i=1}^{n} V_i(Q_i) + \sum_{i<j}^{n} V_{ij}(Q_i, Q_j) + \sum_{i<j<k}^{n} V_{ijk}(Q_i, Q_j, Q_k), \quad (2)$$

where

$$V_i(Q_i) \equiv V(Q_1 = 0, \ldots, Q_i, \ldots, Q_n = 0), \quad (3)$$

$$V_{ij}(Q_{ij}) \equiv V(Q_1 = 0, \ldots, Q_i, \ldots, Q_j, \ldots, Q_n = 0), \quad (4)$$

and

$$V_{ijk}(Q_{ijk}) \equiv V(Q_1 = 0, \ldots, Q_i, \ldots, Q_j, \ldots, Q_k, \ldots, Q_n = 0). \quad (5)$$

Thereby, the PES is expanded along the normal coordinate axes, including up to the three mode coupling representation. Each expansion term includes 11^n grid points, where n is the number of coupled modes. Thus for the $V_{ijk}(Q_i, Q_j, Q_k)$ normal coordinate potential, 1331 grid points were evaluated for each unique combination of mode triplets. The *mb*CO2 function was used to evaluate the single point potential energies at each grid point.

B. Coordinate system

Two separate coordinate systems were exploited in this study: rectilinear Cartesian coordinates and general curvilinear internal coordinates. The reason for the two distinct coordinate frames was to address the different types of vibrational motions. In particular, the large-amplitude floppy motions exhibited by the intermolecular modes are best-suited for a curvilinear description. Conversely, the rigid motions of the intramolecular vibrations can be described straightforwardly by Cartesian coordinates. Furthermore, the degeneracy of bending modes poses problems for the internal coordinate description.[48] The linear structure of the CO_2 molecule results in singularities in the kinetic energy operator of the curvilinear frame Hamiltonian causing the discrete variable approximation to break down. Also in the Cartesian frame, the rovibronic couplings are typically ignored for efficiency; however, neglecting the rovibronic energy levels is not feasible with general internal coordinates.

The rectilinear normal coordinates were computed in terms of mass-weighted Cartesian displacements. This coordinate frame has consistently been shown to reliably treat the intramolecular rigid motions of isolated small molecules. When the interactions between vibrational motions are considered (e.g., with vibrational structure methods), the calculated frequencies closely match experimental band positions.[46] For the energy level calculations of the monomer and the dimer intramolecular vibrations, we employ rectilinear normal coordinates implemented in the SINDO[49,50] and MAVI[51,52] programs.

For the intermolecular dimer frequencies, general curvilinear internal coordinates were employed using the NITROGEN program.[48] The reduced-dimensional treatment of the dimer vibrations is justified due to the small coupling between the intra- and intermolecular modes. This has been remarked on by many previous studies, especially in the case of water molecules,[42–46,53,54] and the same reasoning applies here. The reduction in the number of degrees of freedom also benefits computation efficiency, allowing for the implementation of higher levels of vibrational structure theory.

C. Vibrational Schrödinger equation

The literature describing vibrational structure theory is very thorough, and the reader is directed there for a more exhaustive explanation of the methodology.[49,55–59] A brief introduction is included here as a refresher.

The aforementioned potential energy surfaces (QFF, grid) are included in the following vibrational Hamiltonian:

$$H = -\frac{1}{2}\sum_m \frac{\partial^2}{\partial Q_m^2} + V(\mathbf{Q}). \quad (6)$$

This formalism neglects the rovibrational couplings of the complete Watson Hamiltonian[60] but has proven very effective at accurately addressing the vibrational frequencies of many molecular systems.[50,58,61] Here, we use the vibrational structure formalism within the SINDO[49,50] and the MAVI programs.[51] However, one of the drawbacks of this Hamiltonian is that it performs poorly when computing the large amplitude motions typically found in intermolecular vibrations. For such cases, the complete Watson Hamiltonian is preferred.

Solving the above truncated Hamiltonian and the more complete Watson Hamiltonian can be performed using a suite of vibrational structure methods. The vibrational self-consistent field (VSCF) method[62–65] is inexpensive and exact when the Hamiltonian is additively separable. More accurate vibrational correlation methods, including vibrational second-order Møller-Plesset perturbation theory (VMP2)[50,55,57] and vibrational configuration interaction (VCI),[66–68] explicitly account for the interactions between molecular vibrations. All of these procedures are constructed and implemented in similar ways to their electronic structure counterparts. For instance, the VSCF wavefunction is represented as the product of modes as

$$\Psi_{\mathbf{n}}^{\mathrm{VSCF}}(\mathbf{Q}) = \prod_k \varphi_{n_k}^{(k)}(Q_k), \quad (7)$$

where n_k represents the quantum number of the kth mode. Solving the VSCF equation below yields the one-mode function, $\varphi_{n_k}^{(k)}$, and the energy, $\epsilon_{n_k}^{(k)}$, as

$$\left[-\frac{1}{2}\frac{\partial^2}{\partial Q_k^2} + \left\langle \prod_{i\neq k} \varphi_{n_i}^{(i)} \middle| V \middle| \prod_{j\neq k} \varphi_{n_j}^{(j)} \right\rangle\right] \varphi_{n_k}^{(k)} = \epsilon_{n_k}^{(k)} \varphi_{n_k}^{(k)}. \quad (8)$$

Again since the VSCF approach does not explicitly account for mode-mode coupling, it is typically less accurate than the vibrational correlated methods. Also, it fails to describe phenomena arising from mode-mode coupling, e.g., Fermi resonance. The equations for VMP2 and VCI can be obtained straightforwardly from here and are found elsewhere in the literature.[50,55,57,66–68]

III. RESULTS

A. Monomer

We first present the vibrational structure results of the CO_2 monomer to showcase the spectroscopic accuracy of the *mb*CO2 potential compared to the best available theoretical and experimental data.[4] Previously, the best theoretical estimate[25] was obtained by a mixed QFF and quadrature PES obtained at the CCSD(T) complete basis set extrapolated level of theory with vibrational correlation accounted for by the VCI method. The vibrational frequencies of the isolated CO_2 molecule are outlined in Table I, where

TABLE I. The low-lying vibrational energy levels in cm^{-1} of the CO_2 monomer obtained with the harmonic approximation, VSCF and VCI methods compared to the best theoretical and experimental estimates.

Method	$\nu_2(01^10)$	$\nu_1(10^00)$	$\nu_2^2(02^20)$	$\nu_2^2(02^00)$	$\nu_3(00^01)$
CCSD(T)-F12b/aVQZ/HAR	673.4	1354.4	1346.8	...	2396.4
*mb*CO2/HAR	673.0	1352.2	1346.0	...	2393.4
*mb*CO2/QFF/VSCF	668.5	1340.2	1337.0	...	2350.9
*mb*CO2/grid/VSCF	668.8	1340.4	1341.7	...	2352.0
*mb*CO2/QFF/VCI	667.3	1284.0[a]	1334.6	1388.1[a]	2346.0
*mb*CO2/grid/VCI	667.8	1284.7[a]	1336.9	1388.7[a]	2346.7
Rodriguez-Garcia *et al.*[b]	669.1	1288.9[a]	1339.6	1389.3[a]	2349.2
Expt.[c]	667.4	1285.4[a]	1335.1	1388.2[a]	2349.2

[a]Fermi doublet.
[b]Reference 25.
[c]Reference 4.

results at the VSCF and VCI levels are displayed using both the QFF and quadrature (grid) potential surfaces. The VMP2 results and a more exhaustive set of VSCF and VCI frequencies can be found in the supplementary material.

For the frequencies obtained at the harmonic approximation, the bending and asymmetric stretching modes agree fairly well when compared to experimental results. The difference in energy is less than six wavenumbers for the degenerate bending modes (experimentally observed at 667.8 cm^{-1}) and about 45 wavenumbers for the asymmetric stretch mode (found experimentally at 2349.2 cm^{-1}), which amount to percent errors of just over 2%. The lack of mode-mode coupling in this approximation prohibits the description of Fermi resonance between the symmetric stretch fundamental and bending overtone. Instead, the harmonic approximation results predict the near degeneracies of these energy levels as expected, although the bending overtone agrees well with the unperturbed 02^20 bending overtone found theoretically and experimentally. There is no direct experimental comparison for the symmetric stretch frequency; however, the theoretical best estimate using the VSCF method in Table I of Rodriquez-Garcia *et al.* was found to be 1343.0 cm^{-1}. This frequency is nearly identical to those of the VSCF calculation performed in this work. Both the QFF and quadrature procedures agree to within 4 cm^{-1} at the VSCF level of theory for the symmetric vibration, and this excellent agreement is echoed for the remaining fundamental and overtone frequencies when compared to the experimental and theoretical best estimates. The dyad peaks remain elusive, however, and require a vibrational correlation treatment.

The VCI treatment represents the most complete depiction of the mode-mode coupling of these vibrational motions and shows improved accuracy compared to the harmonic and VSCF results with respect to the experiment. The frequencies computed at this level differ by no more than 4 cm^{-1} from the observed frequencies, even in the high frequency asymmetric stretch region (2346.0 cm^{-1} for QFF and 2346.7 cm^{-1} for grid). This amounts to about 0.1% error for the VCI treatments. The slight improvement in the quadrature procedure is attributed to the accurate description of the monomer PES, where specifically 7825 unique grid points were evaluated. In each VCI approach, since mode correlation is explicitly described, the Fermi resonance phenomenon can be predicted. Two vibrational bands arise from this phenomenon at 1284.0 and 1388.1 cm^{-1} with the QFF potential and at 1284.7 and 1388.7 cm^{-1} with the grid potential. Somewhat fortuitously, these values more closely predict the experimental energy levels than the theoretical best estimate. We assume this is due to error cancellation from lack of basis set completeness. The reader is referred to Fig. 1 in Ref. 25, which shows the convergence of each mode as a function of basis set size. Furthermore, the VCI wavefunctions of the Fermi doublet can be written to show the strength and locality of mode coupling. According to the results using the *mb*CO2 potential and the grid potential approximation, the VCI wavefunctions are described as a linear combination of VSCF wavefunctions as

$$\Psi_{10^00}^{\mathrm{VCI}} = -0.74\Psi_{\nu_1}^{\mathrm{VSCF}} - 0.48(\Psi_{\nu_2^2}^{\mathrm{VSCF}} + \Psi_{\bar{\nu}_2^2}^{\mathrm{VSCF}}), \tag{9}$$

and

$$\Psi_{02^00}^{\mathrm{VCI}} = 0.68\Psi_{\nu_1}^{\mathrm{VSCF}} - 0.52(\Psi_{\nu_2^2}^{\mathrm{VSCF}} + \Psi_{\bar{\nu}_2^2}^{\mathrm{VSCF}}). \tag{10}$$

Here, ν_2 and $\bar{\nu_2}$ are the degenerate bending modes. The contributions from the ν_1 mode to each of the Fermi dyad wavefunctions also helps explain the shared intensity of these vibrational peaks in the Raman spectrum.[69,70] The monomer data highlight not only the systematic improvability of the vibrational structure methods but also of the PES: the harmonic approximation is less accurate than the QFF, which appears slightly less accurate than the quadrature treatment. These facts will be used to accurately predict vibrational energy levels of the intramolecular and intermolecular CO_2 dimer modes.

B. Dimer intermolecular frequencies

For the vibrational motions of the minimum energy dimer, we first focus on the low-frequency intermolecular modes. These degrees of freedom are particularly difficult to describe due to their large-amplitudes and delocalized nature. Nonetheless, their characterization is crucial to understanding the van der Waals interactions in the current system, as well as the combination bands near 2400 cm^{-1}.[19] The four fundamental intermolecular modes are

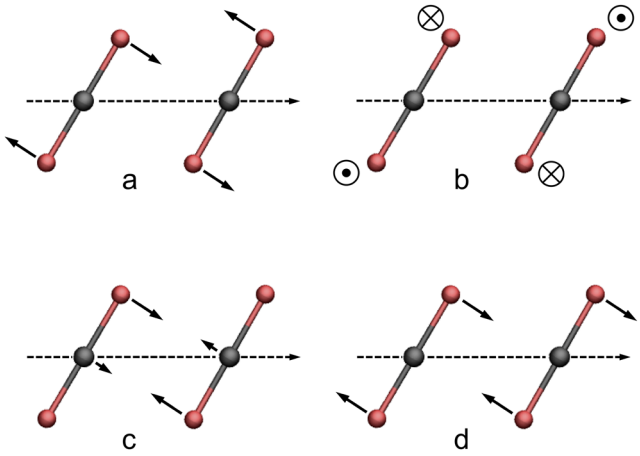

FIG. 2. The four intermolecular fundamental vibrational modes of the CO_2 dimer are shown. The antisymmetric in-plane bend–B_u (a), the out-of-plane torsion–A_u (b), the symmetric van der Waals stretch–A_g (c), and the symmetric in-plane bend–A_g (d) are qualitatively depicted.

shown in Fig. 2 and refer to the antisymmetric in-plane bend (ν_a), the out-of-plane torsion (ν_b), the symmetric van der Waals stretch (ν_c), and the symmetric in-plane bend (ν_d). The vibrational energy levels of relevant modes in this intermolecular region, including combination and overtones, were computed at various levels of theory and reported in Table II alongside the theory and experiment from the literature. The VSCF, VMP2, and complete list of VCI results can be found in the supplementary material.

In Table II, the two lowest frequency modes, the in-plane bend and the out-of-phase torsion (ν_a and ν_b), are found within 4 cm^{-1} of each another across all levels of theory and experiment. The large majority of these reported values place the bending frequency slightly lower in energy; however, the CCSD(T)-F12b/aug-cc-pVQZ and *mb*CO2 harmonic data indicate the opposite ordering. The results at the harmonic level are also significantly blueshifted from the theory and experiment in the literature. The best experimental estimate for these vibrational bands indicate energy levels at 22.26 and 23.24 cm^{-1},[19] which agree remarkably well with our VCI results at 22.6 and 24.2 cm^{-1}, respectively. Also, the energy difference is strikingly similar and slightly improved compared to other theoretical studies.

Next, we consider the most energetic of the fundamental intermolecular vibrations: the symmetric in-plane bend. Experimentally, this mode is found at 92.25 cm^{-1}, and most theoretical results that account for some deviations from the harmonic approximation can reproduce this frequency value to within 3 cm^{-1}. For example, our *mb*CO2/VCI results show an energy of 93.9 cm^{-1} for this vibrational motion. The harmonic approximation, on the other hand, substantially overestimates the frequency of this mode. In particular, the *mb*CO2/HAR result (107.2 cm^{-1}) exhibits a 16% error compared to the experimental value. This fact suggests the significant anharmonicity of this vibrational motion. Furthermore, since the *mb*CO2/VSCF frequency for this mode is 94.12 cm^{-1}, which closely agrees with the experimental result, it appears to exhibit relatively weak coupling with the other motions in the intermolecular region. In fact, the VCI wavefunction confirms this result (see the supplementary material).

Finally, we explore the van der Waals stretch fundamental, ν_c, and the overtone of the antisymmetric in-plane bend, $2\nu_a$. These two modes are grouped together because of their accidental degeneracy, indicated in our VCI results. According to the *mb*CO2/HAR results, the stretching mode has a frequency of 46.2 cm^{-1}, and even though the bend fundamental is found at 30.0 cm^{-1}, placing the overtone frequency near 60.0 cm^{-1}, the CCSD(T)-F12b/aug-cc-pVQZ/HAR and *mb*CO2/VSCF results suggest that this mode is significantly less energetic. In fact, twice the *mb*CO2/VSCF antisymmetric bend frequency amounts to 48.8 cm^{-1}, slightly more energetic than the stretching vibrational energy level. These two modes also share the same A_g symmetry. Thus, strong coupling would be expected as is the case for the Fermi dyad in the CO_2 monomer. And in fact, we see just that: two peaks are observed at 34.4 cm^{-1} and at 49.6 cm^{-1}, according to the *mb*CO2/VCI theory.

TABLE II. The low-lying intermolecular vibrational energy levels in cm^{-1} of the CO_2 dimer obtained with the harmonic approximation, VSCF and VCI methods compared to the experiment and recent theoretical literature. The Fermi dyad peaks are shown as ν_- and ν_+ and are composed mainly of the $2\nu_a$ and ν_c modes.

Assignment	CCSD(T)-F12b/aVQZ HAR	*mb*CO2 HAR	*mb*CO2 VCI	Chen and Light[a]	Wang *et al.*[b]	Expt.[c]
$\nu_a(B_u)$	22.5	30.0	22.6	19.69	20.64	22.26
$\nu_b(A_u)$	19.9	26.6	24.2	22.62	24.44	23.24
$\nu_+(A_g)$	42.2	49.6	48.6	40.84	46.07	...
$\nu_a + \nu_b(B_g)$	...	...	45.5	41.01	43.27	...
$2\nu_b(A_g)$	...	...	47.3	44.35	48.20	...
$\nu_-(A_g)$	...	...	34.4	29.45	32.34	31.509
...	...	...	...	...	...	...
$\nu_d(A_g)$	106.7	107.3	93.9	90	93.23	92.25

[a]Reference 32.
[b]Reference 33.
[c]Reference 19.

This analysis is confirmed by interpreting the VCI wavefunctions of the two motions

$$\Psi_{\nu_-}^{\mathrm{VCI}} = 0.74\Psi_{\nu_c}^{\mathrm{VSCF}} - 0.51\Psi_{2\nu_a}^{\mathrm{VSCF}} + \cdots, \tag{11}$$

and

$$\Psi_{\nu_+}^{\mathrm{VCI}} = 0.58\Psi_{\nu_c}^{\mathrm{VSCF}} + 0.52\Psi_{2\nu_a}^{\mathrm{VSCF}} - 0.39\Psi_{2\nu_b}^{\mathrm{VSCF}} + \cdots. \tag{12}$$

Even though substantial mixing is observed for the ν_- and ν_+ modes, the leading contributions to the VCI wavefunctions of both are the bending overtone and the symmetric stretch fundamental VSCF wavefunctions. This is strikingly similar to the Fermi doublet for the CO_2 monomer. The two main differences here are the magnitude of the splitting and the number of modes that contribute. It should be noted that the VCI wavefunctions in Eqs. (11) and (12) only show VSCF contributions from modes with coefficients above 0.3. Also, care should be taken in interpreting these results since these specific VCI eigenvectors are quite sensitive to small changes in the computation (e.g., the PES, the level of theory, or the separate treatment of intermolecular and intramolecular modes). Additional theoretical investigations would be helpful to confirm these results. However, this mixing has also been observed in other studies and makes combination mode assignment ambiguous.[19,32,33] Since, the ν_c VSCF wavefunction contribution to the ν_- VCI wavefunction is larger than to the ν_+ VCI wavefunction, one could reasonably refer to these modes as the ν_c and $2\nu_a$ modes, respectively. However, we have rejected this characterization due to the substantial mode delocalization and also due to the existing literature classification.

C. Dimer intramolecular frequencies

Finally, we focus on the intramolecular modes of the CO_2 dimer, whose frequencies are shown in Table III. The eight vibrational motions are associated with in-phase and out-of-phase combinations of the four monomer modes. For instance, the two vibrational frequencies in the asymmetric stretching region correspond to motions where the CO_2 molecules are undergoing stretches in-phase and out-of-phase. For the bending modes, two additional categories of motions exist: parallel to the plane of symmetry (para.) and perpendicular to the plane of symmetry (perp.), as depicted in Fig. 3.

Starting with the *mb*CO2 harmonic results, the vibrational frequencies of the dimer correspond well with the frequencies of the monomer, especially if one accounts for the symmetry of the dimer vibrations. That is, when a dimer mode has a similar symmetry to the isolated molecule (e.g., A_g and Σ_g^+), the frequencies coincide. For example, in the asymmetric stretching region, the in-phase mode (B_u symmetry) corresponds nearly exactly to the monomer harmonic vibrational energy level (Σ_u^+ symmetry), 2392.0 cm^{-1} and 2393.4 cm^{-1}, respectively, while the more symmetric out-of-phase mode is observed more than 6 cm^{-1} lower. The in-phase symmetric stretching frequency at 1350.9 cm^{-1} is compared to 1352.2 cm^{-1} for the monomer, while the out-of-phase motion is 10 cm^{-1} lower in energy. The in-phase parallel bend with similar symmetry to the monomer has a nearly identical energy to the monomer motion, 673.4 and 673.0 cm^{-1}, respectively. The remaining bending frequencies show larger deviations. The in-phase perpendicular bend mode appears at 681.3 cm^{-1}, while the out-of-phase parallel and perpendicular bend are found at 672.5 and 668.6 cm^{-1}, respectively.

Next, we present the fundamental VSCF and VCI intramolecular vibrational energy levels with the QFF and grid approximations. These were also calculated at the 3MR level using the VSCF, VMP2, and VCI methodologies, each with a QFF and grid PES. A complete compilation of the results at all levels of theory can be found in the supplementary material. Starting with the asymmetric modes, a redshift of the vibrational frequencies is observed compared to the harmonic counterparts. Also, both potential approximations at the VCI level show less energetic frequencies compared to the monomer. The symmetric stretching fundamental frequencies are less affected by the anharmonic treatment. We focus on the harmonic and VSCF results here due to the Fermi splitting. Both the harmonic and grid results show phase splitting of over 10 cm^{-1} in this region, but the QFF potential splitting is half of that, with values within the range of the harmonic frequencies. Notably, the CCSD(T)-F12b/aVQZ

TABLE III. The intramolecular vibrational energy levels for the CO_2 dimer obtained with the harmonic approximation, VSCF and VCI. Values are shown in cm^{-1}.

Mode	CCSD(T)-F12b/aVQZ Harmonic	*mb*CO2 Harmonic	*mb*CO2 QFF/VSCF	*mb*CO2 Grid/VSCF	*mb*CO2 QFF/VCI	*mb*CO2 Grid/VCI
$\nu_1(B_g)$	671.8	668.6	667.5	667.3	665.3	666.5
$\nu_2(A_g)$	672.4	672.5	670.1	670.3	667.5	671.5
$\nu_3(B_u)$	669.5	673.4	671.3	671.4	668.5	672.5
$\nu_4(A_u)$	675.9	681.3	679.5	679.7	677.3	681.5
$\nu_5(B_u)$	1353.5	1340.0	1329.6	1329.8	1276.5[a]	1280.2[a]
$\nu_6(A_g)$	1353.4	1350.9	1341.1	1341.4	1281.8[a]	1286.7[a]
$\nu_7(B_u)$	...	...	...	...	1386.6[a]	1387.8[a]
$\nu_8(A_g)$	...	...	...	...	1395.5[a]	1399.8[a]
$\nu_9(A_g)$	2392.5	2385.8	2354.3	2355.4	2346.1	2336.0
$\nu_{10}(B_u)$	2397.8	2392.0	2360.6	2361.6	2352.3	2342.2

[a]Fermi doublets.

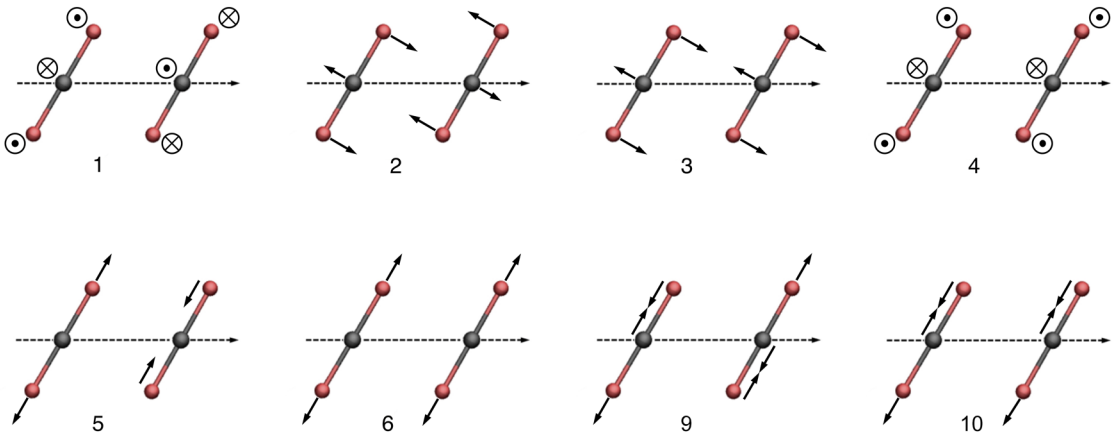

FIG. 3. The eight intramolecular fundamental vibrational modes of the CO_2 dimer are shown. The out-of-phase perpendicular bend–B_g (1), the out-of-phase parallel bend–A_g (2), the in-phase parallel bend–B_u (3), the in-phase perpendicular bend–A_u (4), the out-of-phase symmetric stretch–B_u (5), the in-phase symmetric stretch–A_g (6), the out-of-phase asymmetric stretch–A_g (9), and the in-phase asymmetric stretch–B_u (10) are all qualitatively depicted. The perpendicular and parallel bends are relative to the plane of symmetry.

bending mode frequencies are also consistent with those of the monomer, at all levels of theory. Specifically, the modes are slightly redshifted. The out-of-phase para. bend and the in-phase perp. bend are situated near 674 cm^{-1}, while the out-of-phase perp. bend and the in-phase para. bend are found more than 10 cm^{-1} less near 661 cm^{-1}. The results for the *mb*CO2/grid/VCI show an increase in energy, however. On average, this blueshift amounts to 20 cm^{-1}.

The VCI vibrational energies and wavefunctions again allow for the exploration of the Fermi resonance phenomenon. In particular, the *mb*CO2/grid/VCI wavefunction coefficients [Eqs. (13)–(16)] show the contribution to the dyad peaks from the VSCF wavefunctions

$$\Psi^{\mathrm{VCI}}_{\nu_5} = -0.80\Psi^{\mathrm{VSCF}}_{\nu_5} - 0.47\Psi^{\mathrm{VSCF}}_{\nu_2+\nu_3} - 0.37\Psi^{\mathrm{VSCF}}_{\nu_1+\nu_4} + \cdots, \quad (13)$$

$$\Psi^{\mathrm{VCI}}_{\nu_6} = -0.75\Psi^{\mathrm{VSCF}}_{\nu_6} - 0.37\Psi^{\mathrm{VSCF}}_{2\nu_1} + 0.36\Psi^{\mathrm{VSCF}}_{2\nu_2} + 0.32\Psi^{\mathrm{VSCF}}_{2\nu_3} - 0.25\Psi^{\mathrm{VSCF}}_{2\nu_4} + \cdots, \quad (14)$$

$$\Psi^{\mathrm{VCI}}_{\nu_7} = -0.60\Psi^{\mathrm{VSCF}}_{\nu_5} + 0.60\Psi^{\mathrm{VSCF}}_{\nu_1+\nu_4} + 0.53\Psi^{\mathrm{VSCF}}_{\nu_2+\nu_3} + \cdots, \quad (15)$$

and

$$\Psi^{\mathrm{VCI}}_{\nu_8} = 0.64\Psi^{\mathrm{VSCF}}_{\nu_6} - 0.51\Psi^{\mathrm{VSCF}}_{2\nu_4} + 0.34\Psi^{\mathrm{VSCF}}_{2\nu_3} + 0.34\Psi^{\mathrm{VSCF}}_{2\nu_2} - 0.32\Psi^{\mathrm{VSCF}}_{2\nu_4} + \cdots. \quad (16)$$

For each of the VCI wavefunctions, the symmetric stretch VSCF eigenfunctions are the leading contributions. The A_g symmetry doublet (ν_6 and ν_8) is much more delocalized than the B_u symmetry doublet since significantly more VSCF modes contribute to these peaks. We again stress the sensitivity of these VCI eigenvectors to small changes in the computation and the value of additional theoretical and experimental investigations.

IV. CONCLUSIONS

The *mb*CO2 PEF has been shown to accurately predict the vibrational energy levels, including anharmonic effects, of the CO_2 monomer and dimer. In particular, the agreement with the experiment obtained for the monomer resembles the best theoretical methodology to date and is within a few wavenumbers of the observed frequencies, including the Fermi dyad peaks. The dimer frequencies were separated into the intermolecular and intramolecular motions and were also shown to be accurate compared to the existing experimental data. In the intramolecular region, the vibrational energy levels correspond closely to those of the isolated monomer, and again Fermi resonance is observed for the dimer, this time resulting in a pair of dyads. Notably, the infrared-active asymmetric stretching frequency is redshifted by about 10 cm^{-1}, which could complicate combination mode assignment. However, we assume much of this change in energy is an artifact of the PEF. The intermolecular modes match recently published experimental and theoretical frequencies. However, we are able to show the extent of mixing and delocalization of the intermolecular vibrations through the VCI wavefunction. In particular, the ν_+ and ν_- modes are composed mainly of the van der Waals stretch and antisymmetric in-phase bend overtone VSCF wavefunctions. Thus, the similarities with the Fermi resonance in the monomer and dimer are striking.

Future work on the CO_2 system will focus on the two nearly degenerate trimer isomers. These two experimentally determined structures have been explored experimentally, but few results are currently available for their vibrational spectra. Just as is the case for the dimer, theoretical work is imperative for experimental band assignments in the larger clusters. However, the number of degrees of freedom in these systems pushes the limit of the theoretical methods available. The *mb*CO2 PEF provides a robust and efficient means to determine and validate the vibrational structure for these types of homogeneous CO_2 systems.

SUPPLEMENTARY MATERIAL

See supplementary material for the complete QFF force constants, VSCF, VMP2, and VCI vibrational frequencies. Also, all of the manuscript data, including the supplementary material, can be generated from the author's GitHub repository (https://github.com/sodelab). This repository contains all of the necessary code involved in this manuscript as well as instructions for downloading the other required software.

ACKNOWLEDGMENTS

This research was supported by the National Science Foundation through a subaward (Grant No. ACI-1550588) by the American Chemical Society Petroleum Research Fund (Grant No. 58240-UNI6) and by the Florida Education Fund. Supercomputing time was provided by XSEDE (Grant No. TG-CHE150093) and by the Research Computing Center at The University of Chicago. Also, this research used resources of the Argonne Leadership Computing Facility, which is a DOE Office of Science User Facility supported under Contract No. DE-AC02-06CH11357.

REFERENCES

[1] P. E. Martin and E. F. Barker, Phys. Rev. **41**, 291 (1932).
[2] A. Adel and D. M. Dennison, Phys. Rev. **43**, 716 (1933).
[3] A. Adel and D. M. Dennison, Phys. Rev. **44**, 99 (1933).
[4] A. Chedin, J. Mol. Spectrosc. **76**, 430 (1979).
[5] Y. I. Baranov and A. A. Vigasin, J. Mol. Spectrosc. **193**, 319 (1999).
[6] A. A. Vigasin, Y. I. Baranov, and G. V. Chlenova, J. Mol. Spectrosc. **213**, 51 (2002).
[7] B. P. Stoicheff, Can. J. Phys. **36**, 218 (1958).
[8] G. Amat and M. Pimbert, J. Mol. Spectrosc. **16**, 278 (1965).
[9] M. H. Andrade e Silva and G. Amat, J. Mol. Spectrosc. **29**, 384 (1969).
[10] H. E. Howard-Lock and B. P. Stoicheff, J. Mol. Spectrosc. **37**, 321 (1971).
[11] J. F. Bertrán, Spectrochim. Acta A **39**, 119 (1983).
[12] S. Montero, J. Chem. Phys. **79**, 4091 (1983).
[13] R. E. Miller and R. O. Watts, Chem. Phys. Lett. **105**, 409 (1984).
[14] K. W. Jucks, Z. S. Huang, D. Dayton, R. E. Miller, and W. J. Lafferty, J. Chem. Phys. **86**, 4341 (1987).
[15] M. A. Walsh, T. H. England, T. R. Dyke, and B. J. Howard, Chem. Phys. Lett. **142**, 265 (1987).
[16] A. S. Pine and G. T. Fraser, J. Chem. Phys. **89**, 100 (1988).
[17] T. Konno and Y. Ozaki, Chem. Phys. Lett. **394**, 198 (2004).
[18] M. Dehghany, M. Afshari, N. Moazzen-Ahmadi, and A. R. W. McKellar, J. Chem. Phys. **128**, 064308 (2008).
[19] J. N. Oliaee, M. Dehghany, M. Rezaei, A. R. W. McKellar, and N. Moazzen-Ahmadi, J. Chem. Phys. **145**, 174302 (2016).
[20] W. D. Allen, Y. Yamaguchi, A. G. Császár, D. A. Clabo, Jr., R. B. Remington, and H. F. Schaefer III, Chem. Phys. **145**, 427 (1990).
[21] P. E. Maslen, D. Jayatilaka, S. M. Colwell, R. D. Amos, and N. C. Handy, J. Chem. Phys. **95**, 7409 (1991).
[22] J. M. L. Martin, P. R. Taylor, and T. J. Lee, Chem. Phys. Lett. **205**, 535 (1993).
[23] H. P. Martins Filho, Spectrochim. Acta, Part A **58**, 2621 (2002).
[24] G. Czakó, T. Furtenbacher, A. G. Császár, and V. Szalay, Mol. Phys. **102**, 2411 (2004).
[25] V. Rodriguez-Garcia, S. Hirata, K. Yagi, K. Hirao, T. Taketsugu, I. Schweigert, and M. Tasumi, J. Chem. Phys. **126**, 124303 (2007).
[26] C. S. Murthy, K. Singer, and I. R. McDonald, Mol. Phys. **44**, 135 (1981).
[27] S. Tsuzuki, T. Uchimaru, K. Tanabe, S. Kuwajima, N. Tajima, and T. Hirano, J. Phys. Chem. **100**, 4400 (1996).
[28] M. Welker, G. Steinebrunner, J. Solca, and H. Huber, Chem. Phys. **213**, 253 (1996).
[29] H.-S. Lee, H. Chen, and J. C. Light, J. Chem. Phys. **119**, 4187 (2003).
[30] Y. N. Kalugina, I. A. Buryak, Y. Ajili, A. A. Vigasin, N. E. Jaidane, and M. Hochlaf, J. Chem. Phys. **140**, 234310 (2014).
[31] R. Bukowski, J. Sadlej, B. Jeziorski, P. Jankowski, K. Szalewicz, S. A. Kucharski, H. L. Williams, and B. M. Rice, J. Chem. Phys. **110**, 3785 (1999).
[32] H. Chen and J. C. Light, J. Chem. Phys. **112**, 5070 (2000).
[33] X.-G. Wang, T. Carrington, Jr., and R. Dawes, J. Mol. Spectrosc. **330**, 179 (2016).
[34] O. Sode and J. N. Cherry, J. Comput. Chem. **38**, 2763 (2017).
[35] G. A. Cisneros, K. T. Wikfeldt, L. Ojamäe, J. Lu, Y. Xu, H. Torabifard, A. P. Bartók, G. Csányi, V. Molinero, and F. Paesani, Chem. Rev. **116**, 7501 (2016).
[36] G. R. Medders, A. W. Götz, M. A. Morales, P. Bajaj, and F. Paesani, J. Chem. Phys. **143**, 104102 (2015).
[37] V. Babin, C. Leforestier, and F. Paesani, J. Chem. Theory Comput. **9**, 5395 (2013).
[38] G. R. Medders, V. Babin, and F. Paesani, J. Chem. Theory Comput. **10**, 2906 (2014).
[39] V. Babin, G. R. Medders, and F. Paesani, J. Chem. Theory Comput. **10**, 1599 (2014).
[40] M. Majumder, S. E. Hegger, R. Dawes, S. Manzhos, X.-G. Wang, C. Tucker, Jr., J. Li, and H. Guo, Mol. Phys. **113**, 1823 (2015).
[41] Z. Xie and J. M. Bowman, J. Chem. Theory Comput. **6**, 26 (2009).
[42] G. R. Low and H. G. Kjaergaard, J. Chem. Phys. **110**, 9104 (1999).
[43] Y. Wang, S. Carter, B. J. Braams, and J. M. Bowman, J. Chem. Phys. **128**, 071101 (2008).
[44] Y. Watanabe, S. Maeda, and K. Ohno, J. Chem. Phys. **129**, 074315 (2008).
[45] Y. Wang and J. M. Bowman, Chem. Phys. Lett. **491**, 1 (2010).
[46] K. Yagi, M. Keçeli, and S. Hirata, J. Chem. Phys. **137**, 204118 (2012).
[47] H. J. Werner, P. J. Knowles, G. Knizia, F. R. Manby, M. Schütz, P. Celani, W. Györffy, D. Kats, T. Korona, R. Lindh, A. Mitrushenkov, G. Rauhut, K. R. Shamasundar, T. B. Adler, R. D. Amos, A. Bernhardsson, A. Berning, D. L. Cooper, M. J. O. Deegan, A. J. Dobbyn, F. Eckert, E. Goll, C. Hampel, A. Hesselmann, G. Hetzer, T. Hrenar, G. Jansen, C. Köppl, Y. Liu, A. W. Lloyd, R. A. Mata, A. J. May, S. J. McNicholas, W. Meyer, M. E. Mura, A. Nicklass, D. P. O'Neill, P. Palmieri, D. Peng, K. Pflüger, R. Pitzer, M. Reiher, T. Shiozaki, H. Stoll, A. J. Stone, R. Tarroni, T. Thorsteinsson, and M. Wang, MOLPRO, version 2015.1, a package of *ab initio* programs, 2015, see http://www.molpro.net.
[48] P. B. Changala, NITROGEN, Numerical and Iterative Techniques for Rovibronic Energies with General Internal Coordinates, http://www.colorado.edu/nitrogen, 2018.
[49] K. Yagi, K. Hirao, T. Taketsugu, M. W. Schmidt, and M. S. Gordon, J. Chem. Phys. **121**, 1383 (2004).
[50] K. Yagi, S. Hirata, and K. Hirao, Phys. Chem. Chem. Phys. **10**, 1781 (2008).
[51] M. Keçeli and S. Hirata, J. Chem. Phys. **135**, 134108 (2011).
[52] M. Keçeli, MaVi, https://github.com/keceli/MaVi, 2016.
[53] D. P. Schofield and H. G. Kjaergaard, Phys. Chem. Chem. Phys. **5**, 3100 (2003).
[54] T. Salmi, V. Hänninen, A. L. Garden, H. G. Kjaergaard, J. Tennyson, and L. Halonen, J. Phys. Chem. A **112**, 6305 (2008).
[55] L. S. Norris, M. A. Ratner, A. E. Roitberg, and R. B. Gerber, J. Chem. Phys. **105**, 11261 (1996).
[56] G. M. Chaban, J. O. Jung, and R. B. Gerber, J. Chem. Phys. **111**, 1823 (1999).
[57] O. Christiansen, J. Chem. Phys. **119**, 5773 (2003).
[58] O. Christiansen, Phys. Chem. Chem. Phys. **9**, 2942 (2007).
[59] M. Keçeli, T. Shiozaki, K. Yagi, and S. Hirata, Mol. Phys. **107**, 1283 (2009).
[60] J. K. G. Watson, Mol. Phys. **15**, 479 (1968).

[61] J. M. Bowman, S. Carter, and X. Huang, Int. Rev. Phys. Chem. **22**, 533 (2003).
[62] J. M. Bowman, J. Chem. Phys. **68**, 608 (1978).
[63] R. B. Gerber and M. A. Ratner, Chem. Phys. Lett. **68**, 195 (1979).
[64] J. M. Bowman, Acc. Chem. Res. **19**, 202 (1986).
[65] M. A. Ratner and R. B. Gerber, J. Phys. Chem. **90**, 20 (1986).
[66] K. M. Christoffel and J. M. Bowman, Chem. Phys. Lett. **85**, 220 (1982).
[67] G. Rauhut, J. Chem. Phys. **127**, 184109 (2007).
[68] Y. Scribano and D. M. Benoit, Chem. Phys. Lett. **458**, 384 (2008).
[69] K. D. Bier and H. J. Jodl, J. Chem. Phys. **86**, 4406 (1987).
[70] R. C. Hanson, J. Chem. Phys. **75**, 1102 (1981).